# Impact of carbonyl formation on cobalt ripening over Titania surface

Kevin K. B. Duff
*TCM Group, Cavendish Laboratory, University of Cambridge, UK CB3 0HE*

Leonardo Spanu
*Shell India Markets Private Limited, Bangalore, 560048, India*

Nicholas D. M. Hine
*Department of Physics, University of Warwick, Coventry, UK CV4 7AL*
(Dated: April 13, 2017)

We have performed density functional theory calculations of the adsorption and migration energies of different cobalt moieties on anatase surface (101). Surface diffusion of active metal sites is a crucial step in the ripening mechanism, one the primary causes for the loss of active surface area of cobalt Fischer-Tropsch catalyst. Our main objective is to clarify the impact of gas phase molecules on the transport properties of surface-adsorbed cobalt. Water molecule physisorbed to the (101) surface have a negligible impact of the adsorption and diffusion of cobalt ions. On the contrary, cobalt carbonyl species have the largest effect on the energetics of adsorption and surface diffusion. The formation of $Co(CO)_3$ is favourable in realistic reactor conditions and drastically decreases the surface binding energy, making transport via gas phase an alternative viable pathways for cobalt mobility.

## I. INTRODUCTION

Sintering is one of the possible deactivation pathways of transition metal catalysts [1, 2] and is believed to affect Fischer-Tropsch (FT) catalysts particularly in the first few weeks of the catalyst lifetime [3]. Sintering is made up of two distinct processes that act to reduce active surface area: coalescence, which is the motion of large nanoparticles across the surface, and ripening, which is the breaking off, surface diffusion, and recombination of small catalyst particles. Of these, the latter is particularly difficult to probe experimentally*in situ*. This poses a challenge in the identification of factors that may be accelerating ripening, and motivates an alternative computational approach.

The formation, growth, mobility, and interactions of catalytic transition metal atoms and clusters on metal oxide supports have been widely studied both experimentally and computationally using DFT. Examples cover Co [4], Ni [5], Pd [6–12], Ag [10], Pt [10, 13–19], and Au [17, 20–22] on both anatase and rutile $TiO_2$ and Ni [23], Cu [24], Pd [24–26], Ag [1, 27], Pt [28, 29] and others [30] on alumina.

To relate the results of DFT calculations to experimentally-relevant quantities such as macroscopic diffusion coefficients of adsorbate on a surface, a random walk model can be parameterised using adsorption and transition state energies [31]. Even in more complicated surfaces, where there may be more than one unique adsorption site, such as is the case for anatase (101) surface, these energies remain central to describing surface diffusion [32]. This motivates the comparison of absorption and transition state energies for a range of cobalt-containing adsorbates on the support surface as a measure of surface mobility.

In the environment of a Fischer-Tropsch reactor, the catalyst surface is exposed to a range of gas-phase species, any of which may be the determining factor to cobalt transport, and thus to ripening. These include the reactants and gas-phase products of the process and their derivatives. Several of these species can bind to surface-adsorbed cobalt and affect its adsorption and mobility properties. As water is produced as a product, surface-adsorbed water molecules can affect both adsorption and mobility, as well as the formation of surface species. In this article, we aim to study adsorption and diffusion of all potentially relevant species, so as to identify which gas-phase species present in a Fischer-Tropsch reactor are most active in the ripening process.

We focus in particular on three main quantities derived from DFT-based total energy differences between different systems: the absorption energy $\Delta E_{\mathrm{bind}}$, the migration barrier $\Delta E_{\mathrm{mig}}$, and the formation energy $\Delta E_{\mathrm{form}}$. All DFT calculations are performed for cobalt adatoms on anatase $TiO_2$ (101) surface, in presence of different absorbates from gas-phase species (O, CO, and OH groups). The Wulff construction of anatase $TiO_2$ indicates in fact that the (101) surface is dominant, with (001) expected to form as a secondary surface [33]. In the case of anatase (101) water molecules adsorb non-dissociatively [34] and we have therefore considered both dry surface and water covered (1 monolayer, (ML)) case, to clarify the role of water on the surface mobility.

The addition of water to the surface does not significantly affect the energetics of atomic cobalt adsorption on the surface. However we find strong evidence that cobalt carbonyl can be expected to play a crucial role in the overall balance of cobalt transport. The overall contribution of a species to cobalt mobility depends in fact on multiple factors: the binding of the species to the surface, the ability of the species to diffuse across the surface, and the concentration of the species on the

surface.

## II. METHODS

### A. Adsorption, Mobility and Formation Energies

The adsorption energy of a species on a surface is defined in Equation 1 as the energy required to completely remove a bonded instance of that species from the surface and return the surface to its pristine state. This is calculated as a difference in the total energies of three systems:

$$\Delta E_{\text{bind}} = E_{\text{ads}} + E_{\text{slab}} - E_{\text{slab+ads}} \quad (1)$$

Here, $E_{\text{slab+ads}}$ is the total energy of the surface with the adsorbate, $E_{\text{surf}}$ is the total energy of the pristine surface, and $E_{\text{ads}}$ is the total energy of an isolated adsorbate in vacuum.

Given two adsorption sites, a transition state between them can be identified using the nudged elastic band (NEB) method [35, 36]. The energy of this transition state relative to the starting site defines the migration barrier. NEB is a chain-of-states method in which several intermediate images are connected with springs of natural length 0 and relaxed, with the spring force perpendicular to the path and the real force parallel to the path projected out. This relaxation is not global and depends on the choice of initial path, which must be considered carefully where the transition involves many coordinated processes. However for the relatively simple case of the surface motion of an adsorbate with a single surface contact, this is a minor concern, and linear interpolation can be used to construct a sensible initial path.

The formation energy expresses the energy cost to form the adsorbate system relative to the constituent species existing in realistic 'reservoir' conditions within a reactor vessel. We use an approach similar to that of Finnis *et al.* [37, 38] in our definitions of the chemical potentials of the reservoir species, and we use this particularly to estimate formation energies of cobalt carbonyl adsorbates under reactor conditions. In this approach we consider the surface-adsorbed cobalt carbonyl to be in equilibrium with a bath of the CO feedstock at a selected temperature and partial pressure representative of realistic conditions. The formation energy $E_{\text{form}}$ of a species $\text{Co(CO)}_n$ on the anatase surface can be expressed as in Equation 2 in terms of the total energies of the adsorbed species and the chemical potential of the gas-phase species $\mu_{\text{CO}}$.

$$E_{\text{form}} = E_{\text{slab+Co(CO)}_n} - E_{\text{slab+Co}} - n\mu_{\text{CO}}(T, p_{\text{CO}}) \quad (2)$$

The chemical potential of the gas-phase species at a given temperature and partial pressure can be approximated by applying thermodynamics relations of an ideal gas of rigid dumbbells to the experimental Gibbs free energy of formation at standard conditions. A discussion of our calculation of these values without requiring DFT calculations on gas-phase species is provided in the supplementary information. The supplementary information also provides details of DFT calculations on bulk materials used here and elsewhere.

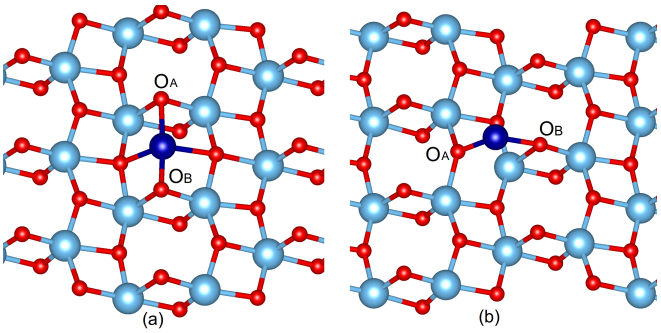


FIG. 1. Adsorption sites of atomic cobalt on the anatase (101) surface. (a) site A is the strongest adsorption site and (b) site B is a second, weaker adsorption site.

### B. Computational Details

Calculations were carried out using the plane-wave DFT package VASP [39–42]. This utilises the PAW method, with standard PAW datasets retaining 17, 12, 6, 4, and 1 electrons respectively in the valence for Co, Ti, O, C and H. The PBE exchange-correlation functional was used for all calculations [43, 44]. It was determined that special treatments of metallic or highly correlated systems were not required as Bader charge analysis [45] indicates the adsorbed cobalt remains in a +2 oxidation state on the surface with only partial reduction in some cases, typically when under-coordinated (See supplementary information for details).

The model surface used throughout consisted of a 4-layer $2 \times 2$ slab of the (101) surface with 14 Å of vacuum. A $2 \times 2 \times 1$ gamma-centred Monkhorst Pack grid was used for $k$-point sampling on surfaces, equivalent to a $4 \times 4 \times 1$ grid on the primitive surface or a $k$-point grid spacing of $0.098\,\text{Å}^{-1}$ by $0.131\,\text{Å}^{-1}$ by $0.037\,\text{Å}^{-1}$. For all calculations a plane-wave cut-off energy of 400 eV was applied. The lowest layer of 24 atoms was held fixed in the bulk structure at all times.

We identify two main sites where adsorption is expected to be favourable for Co: the most favourable, which we call site A, is located between two oxygen atoms on a ridge, with a further two oxygen atoms relatively nearby, as shown in Fig 1(a). However, some adsorbates also bind strongly at a second site, which we call site B, as shown in Fig 1(b). This site also enables bonding of the Co to two nearby oxygen atoms.

We construct geometry models comprising a single Co ion and a Co ion with various functional groups adsorbed at each of these sites. The groups considered are -O, -CO and -OH, which can all easily be formed from the

products or reactants of the FT process.

In practice the surface is rarely dry under reaction conditions, and because of the relatively strong interaction of the 5-fold coordinated surface titanium atoms with water molecules, the geometry of a single monolayer (ML) coverage is relatively stable and partially ordered [46, 47].

The geometry of 1ML coverage of water on the surface is known from previous calculations [48], allowing for the effect of surface hydration to be considered. To this end a second model surface is constructed for the 1ML hydrated surface, and calculations repeated for each of the species adsorbed on this surface. Where necessary, water molecules attached to the surface are moved or removed to make way for the Co-containing species.

Using the relaxed configurations as beginning and end points, we then use the VTST [49, 50] climbing-image NEB functionality for VASP to determine diffusion barriers between the adsorption sites on the surface. These are defined as the difference between the minimum and maximum points on the continuous pathway between two sites which has the lowest overall maximum energy.

In addition to comparing different species, we consider the effect on surface adsorption of adding multiple groups to the Co atom. We do this by forming $Co(CO)_2$ and $Co(CO)_3$ on the dry surface. A mobility study is also performed to examine the effect on surface mobility of additional groups.

## III. RESULTS

### A. Dry Surface Adsorption

Figure 2 depicts the adsorption energies $E_{ads}$ of several different species that can be formed from interactions between a surface-adsorbed cobalt atom and the reactor environment. In each case, the adsorption is made stronger by the the availability of four O atoms for the Co atom to coordinate with, including the four immediately available at site A and the two at site B. In some cases it is also strengthened by the sharing of the functional group with the exposed Ti atom near site A. For example, the site A configuration of CoO shown in Figure 3 has the oxygen coordinating a surface Ti, leading to an overall stronger adsorption. The site B position does not have the same features and limits Co–O coordination, resulting in a much lower adsorption energy.

The addition of further gas molecules species to the adsorbate continues to decrease coordination to surface O atoms, as demonstrated by CoCO, $Co(CO)_2$, and $Co(CO)_3$. Figure 4 depicts the site A adsorption configuration of each of these species. In this case the CO groups do not interact with the surface and this decreased Co surface coordination accompanies a decrease in adsorption energy. No adsorbed configuration for further cobalt carbonyls were found.

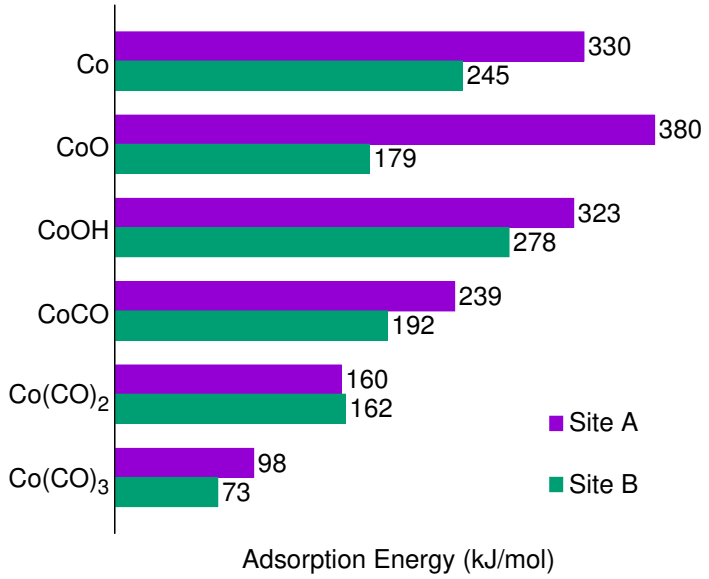


FIG. 2. Adsorption energies of adsorbates on the anatase (101) surface as defined in Equation 1.

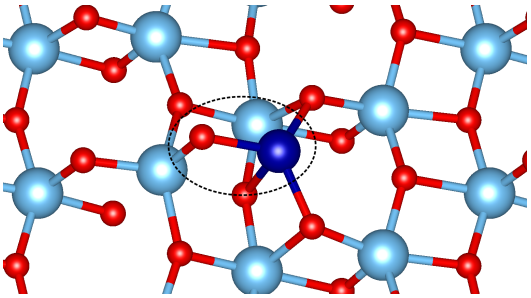

FIG. 3. CoO adsorbed at site A of the $TiO_2$ surface, identified by a circle. While the added O atom decreases the surface coordination of the Co atom, it also coordinates with an exposed Ti atom on the surface. The net effect is a stronger surface adsorption than that of atomic Co.

### B. Dry Surface Mobility

Adsorbate mobility on the surface is central to the ripening process. We have investigated the energy barrier to motion between sites A and B using the nudged elastic band method. The NEB chain was initialized by linear interpolation of the atomic positions between sites A and B along the path rotating around atom $O_A$ as labelled in figure 1(a) and 1(b). While this single path does not provide enough information to create a model of full surface diffusion, it does indicate how the inclusion of various species may affect adsorbate mobility. Figure 5 shows the maximum energy along the NEB path relative to the energy at site A for a number of adsorbates.

The strong surface interaction observed in CoO leads to a large barrier to mobility across the surface com-

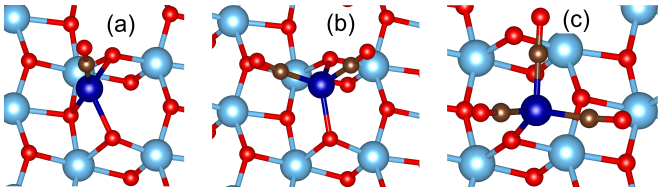


FIG. 4. Site A adsorption configurations of (a) CoCO (b) $Co(CO)_2$ and (c) $Co(CO)_3$ on the (101) anatase surface.

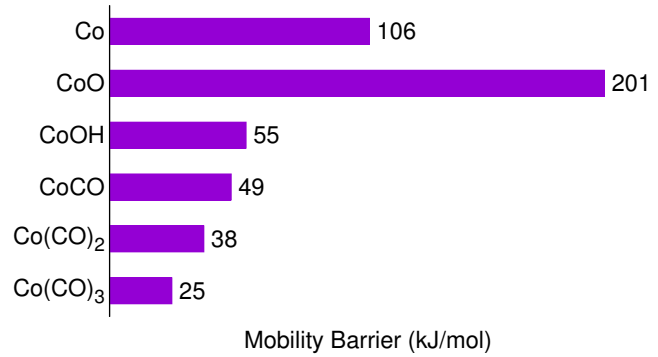


FIG. 5. NEB mobility barriers on the path between sites A and B for adsorbates on the anatase (101) surface.

pared to other adsorbates. However the barrier is approximately halved in CoCO and CoOH. The addition of another carbonyl group further decreases the barrier, potentially due to the decreased cost of partially desorbing from the surface. $Co(CO)_3$ has a mobility barrier that is essentially just the difference in adsorption energies at sites A and B.

### C. Effects of Surface Hydration

Water is produced by the Fischer Tropsch process and is able to bind to the carrier surface. The structure of thin water layers on the anatase (101) surface has been previously investigated [51]. The presence of water can affect the adsorption and mobility of molecules involved in ripening. Figure 6 shows the adsorbed configuration of cobalt at sites A and B of the hydrated surface. Figure 7 contains the adsorption energies $E_{\text{ads}}$ of a selection of the species investigated on a surface with a single monolayer (ML) of water coverage.

Neither CoO nor CoOH were found to have stable adsorbed configurations. Both species induced splitting of a molecule of the water layer to form a surface-adsorbed OH group. Figure 8 shows the configuration of CoOH at site A as a water molecule and a surface-adsorbed cobalt atom. Figure 9 shows the configuration of a CoO at site B as a CoOH molecule. This indicates that the strong interactions between these adsorbates and the water present in the reactor may limit their lifetime and contribution

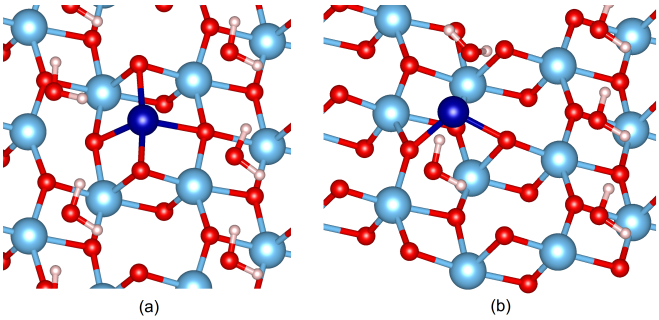


FIG. 6. Adsorbed configuration of a cobalt atom at (a) site A and (b) site B on the monolayer-hydrated anatase (101) surface.

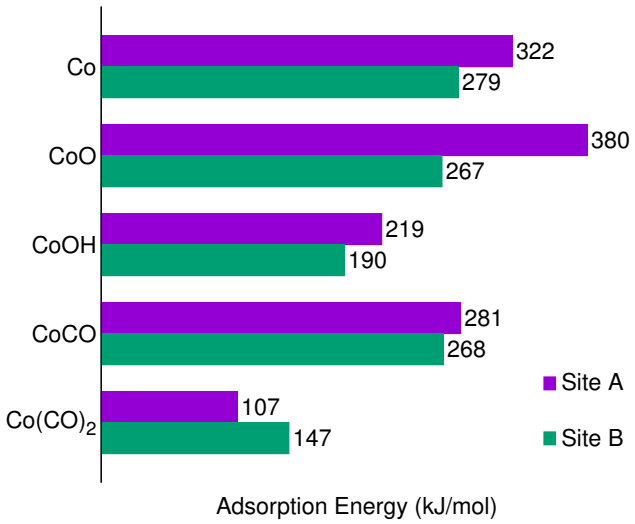


FIG. 7. Adsorption energies of adsorbates on the 1ML hydrated anatase (101) surface as defined in Equation 1.

to Co mobility. Because of the lack of stable adsorbed configurations no migration barriers are reported in these cases.

The addition of water to the surface does not significantly affect the adsorption energies of Co and CoCO, though it does change the surface O coordination of CoCO slightly. Reductions are seen from 330 kJ mol$^{-1}$ to 322 kJ mol$^{-1}$, and from 239 kJ mol$^{-1}$ to 219 kJ mol$^{-1}$ respectively. Migration barriers for these two species were also investigated and again slight reductions from the dry results were found: 106 kJ mol$^{-1}$ to 103 kJ mol$^{-1}$ and 49 kJ mol$^{-1}$ to 36 kJ mol$^{-1}$ respectively. The presence of CO therefore still has a strong impact on Co mobility in the presence of surface hydration.

The adsorption and migration of $Co(CO)_2$ was also investigated, where a significant reduction of site A adsorption energy was found. The mobility barrier was determined to be very small, at approximately 0.75 kJ mol$^{-1}$, noting that the B-A barrier is somewhat higher due to

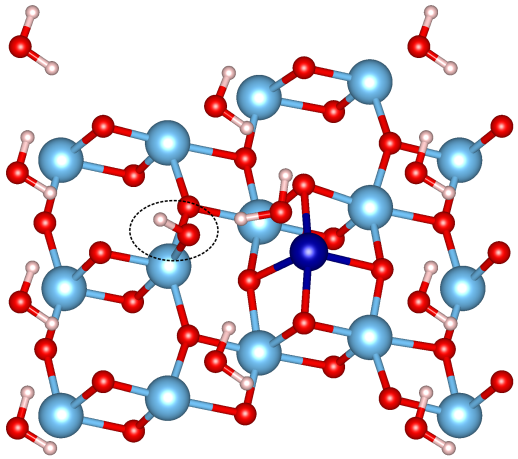

FIG. 8. Geometry of CoOH at site A of the hydrated surface. The adsorbate interacted with the water monolayer to form atomic Co at its adsorption site. The dotted circle identifies the surface-adsorbed OH group that provided a H atom.

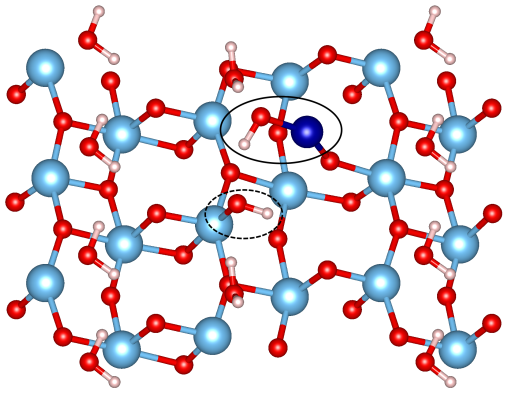

FIG. 9. Geometry of CoO at site B of the hydrated surface. The adsorbate interacted with the water monolayer to form CoOH. The solid circle identifies the adsorbed CoOH molecule. The dotted circle identifies the surface-adsorbed OH group that provided a H atom.

do the difference in adsorption energies. An intermediate state was also found that could not be classified into site A or B and that had a higher adsorption energy of approximately 155 kJ mol$^{-1}$. This indicates the possibility of deeper effects of water coverage on adsorption and mobility that are beyond the scope of this study, which only considers simple translational motion and not any chemically distinct intermediates or the effect of coordinated motion of the adsorbate and water molecules. Because of this limitation the adsorption and migration barrier of $Co(CO)_3$ on the hydrated surface was not studied.

### D. Gas Phase vs. Surface Transport of Carbonyls

Desorption into the gas phase and subsequent re-adsorption to the surface is a cobalt transport method that can compete with surface motion in species with low adsorption energy. The larger carbonyl species investigated have particularly low adsorption energies at certain points on the surface, indicating that if they form in significant quantities on the surface gas phase transport will likely be a competing process in sintering.

We therefore investigate the formation energies of the various cobalt carbonyl species from surface-adsorbed cobalt at site A, as described in the reaction in Equation 3. Figure 10 shows formation energies parameterised to match conditions in a reactor at 500 K in equilibrium with CO gas.

$$Co_{(surf)} + (CO)_{n(g)} \longrightarrow Co(CO)_{n(surf)} \qquad (3)$$

Standard thermochemistry data for the CO gas and the CoO solid were obtained from the NIST Chemistry Webbook [52, 53]. Chemical potentials of CoO and Co bulk crystals and graphitic carbon were obtained using total energy calculations in VASP.

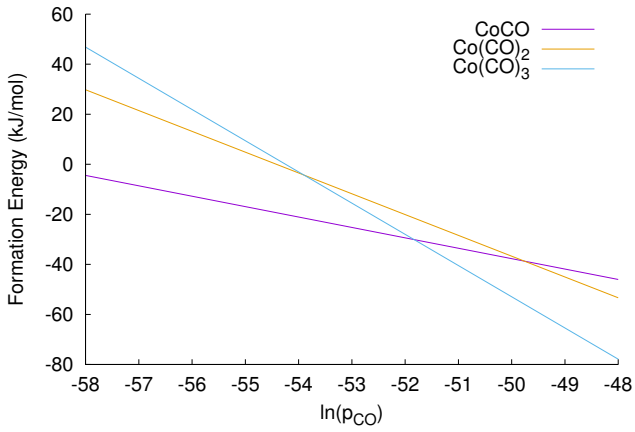


FIG. 10. Formation energy of several species from surface-adsorbed atomic cobalt at site A in equilibrium with a gas-phase CO environment at 500 K. Pressures are in atm.

These results indicate that $Co(CO)_3$ is very dramatically the most favourable species at all realistic reactor conditions. In fact, CoCO only becomes preferred at unrealistically low partial pressures, under $3 \times 10^{-23}$ atm. At 10 atm $Co(CO)_3$ remains favourable up to temperatures exceeding 1500 K. It can therefore be expected to form in conditions where atomic cobalt exists on the surface in contact with CO feedstock.

## IV. DISCUSSION

The relatively high adsorption energy of atomic Co on the (101) anatase surface compared to those of other

cobalt compounds that may form indicate that reactor species can have a strong impact on the ripening process. While there is a significant migration barrier between sites A and B for an isolated cobalt atom, this barrier is, with the exception of CoO, systematically lowered by the inclusion of gas-phase species from the reactor. These effects can be largely attributed to the a decrease in Co coordination with the surface.

The hydrated surface more realistically describes reactor conditions. Based on the stability of OH group formation on the surface it was determined that the water coverage is able to break down CoO and CoOH. While this does not provide information about the likelihood of this event, it can be expected that these species will not be able to continue diffusing over large time scales, and thus are unlikely candidates to contribute significantly to sintering by surface transport. The cobalt carbonyl did not chemically interact with the water molecules or the surface and maintained a low migration energy barrier. Additionally, the carbonyl species had a significantly lower adsorption energies on both the dry and wet surfaces compared to Co, providing a favourable approach to gas-phase transport.

Thermodynamic considerations indicate that in typical reactor conditions the surface formation of cobalt carbonyls, in particular the weakly-adosrbed $Co(CO)_3$, from the CO feedstock is favourable at all realistic reactor conditions. It is therefore believed that both surface and gas-phase transport of the larger cobalt carbonyls are relevant to sintering.

## V. CONCLUSIONS

We have presented a study of the energetics of Co-containing species that could be found on the surface of a typical catalyst support in a Fischer-Tropsch reactor. We have shown that both adsorption energies and surface mobility barriers of these species vary, indicating a link to the ripening process. In particular, carbon monoxide feed binding leading to the formation of mobile cobalt carbonyls has been identified as a candidate for accelerating the ripening process. Gas-phase transport is also viable given the low adsorption energy of the large carbonyls.

This link to the ripening process motivates the study of the adsorption and mobility of small Co clusters in the presence of water and CO. It also motivates the study of the removal of atoms from Co nanoparticle surfaces, edges, and corners in the presence of reactor species. An ongoing study into larger cobalt clusters on anatase surfaces is being performed by our group. It also motivates experimental explorations into the existence of cobalt carbonyl molecules in the product of these reactors.

[1] Meyer, R.; Ge, Q.; Lockemeyer, J.; Yeates, R.; Lemanski, M.; Reinalda, D.; Neurock, M. *Surf. Sci.* **2007**, *601*, 134–145.

[2] Hoflund, G. B.; Minahan, D. M. *J. Catal.* **1996**, *162*, 48–53.

[3] Rytter, E.; Holmen, A. *Catalysts* **2015**, *5*, 478–499.

[4] Galhenage, R. P.; Yan, H.; Tenney, S. A.; Park, N.; Henkelman, G.; Albrecht, P.; Mullins, D. R.; Chen, D. A. *J. Phys. Chem. C* **2013**, *117*, 7191–7201.

[5] Wang, Y.; Su, Y.; Zhu, M.; Kang, L. *RSC Adv.* **2015**, *5*, 16582–16591.

[6] Zhao, W.; Lin, H.; Li, Y.; Zhang, Y.; Huang, X.; Chen, W. *J. Nat. Gas Chem.* **2012**, *21*, 544–555.

[7] Ong, S. V.; Khanna, S. N. *J. Phys. Chem. C* **2012**, *116*, 3105–3111.

[8] Sanz, J. F.; Márquez, A. *J. Phys. Chem. C* **2007**, *111*, 3949–3955.

[9] Zhang, J.; Zhang, M.; Han, Y.; Li, W.; Meng, X.; Zong, B. *J. Phys. Chem. C* **2008**, *112*, 19506–19515.

[10] Pan, X.; Xu, Y.-J. *J. Phys. Chem. C* **2013**, *117*, 17996–18005.

[11] Xu, C.; Lai, X.; Zajac, G. W.; Goodman, D. W. *Phys. Rev. B* **1997**, *56*, 13464–13482.

[12] Negra, M. D.; Nicolaisen, M. N.; Li, Z.; Møller, P. J. *Surf. Sci.* **2003**, *540*, 117–128.

[13] Jiang, D.-e.; Overbury, S. H.; Dai, S. *J. Phys. Chem. C* **2012**, *116*, 21880–21885.

[14] Rieboldt, F.; Vilhelmsen, L. B.; Koust, S.; Lauritsen, J. V.; Helveg, S.; Lammich, L.; Besenbacher, F.; Hammer, B.; Wendt, S. *J. Chem. Phys.* **2014**, *141*, 214702.

[15] Çakir, D.; Gülseren, O. *J. Phys. Chem. C* **2012**, *116*, 5735–5746.

[16] Han, Y.; Liu, C.-j.; Ge, Q. *J. Phys. Chem. B* **2006**, *110*, 7463–7472.

[17] Gong, X.-Q.; Selloni, A.; Dulub, O.; Jacobson, P.; Diebold, U. *J. Am. Chem. Soc.* **2008**, *130*, 370–381.

[18] Zhou, Y.; Muhich, C. L.; Neltner, B. T.; Weimer, A. W.; Musgrave, C. B. *J. Phys. Chem. C* **2012**, *116*, 12114–12123.

[19] Han, Y.; Liu, C.-j.; Ge, Q. *J. Phys. Chem. C* **2007**, *111*, 16397–16404.

[20] Vittadini, A.; Selloni, A. *J. Chem. Phys.* **2002**, *117*, 353–361.

[21] Zhang, L.; Cosandey, F.; Persaud, R.; Madey, T. E. *Surf. Sci.* **1999**, *439*, 73–85.

[22] Chen, Y.; Tian, G.; Pan, K.; Tian, C.; Zhou, J.; Zhou, W.; Ren, Z.; Fu, H. *J. Chem. Soc., Dalton Trans.* **2012**, *41*, 1020–1026.

[23] Parizotto, N.; Rocha, K.; Damyanova, S.; Passos, F.; Zanchet, D.; Marques, C.; Bueno, J. *Appl. Catal., A* **2007**, *330*, 12–22.

[24] Łodziana, Z.; Nørskov, J. K. *J. Chem. Phys.* **2001**, *115*, 11261–11267.

[25] Corral Valero, M.; Digne, M.; Sautet, P.; Raybaud, P. *Oil Gas Sci. Technol.* **2006**, *61*, 535–545.

[26] Corral Valero, M.; Raybaud, P.; Philippe, S. *J. Phys. Chem. B* **2006**, *110*, 1759–1767.

[27] Meyer, R.; Lockemeyer, J.; Yeates, R.; Lemanski, M.; Reinalda, D.; Neurock, M. *Chem. Phys. Lett.* **2007**, *449*, 155–159.

[28] Phatak, A.; Koryabkina, N.; Rai, S.; Ratts, J.; Ruettinger, W.; Farrauto, R.; Blau, G.; Delgass, W.; Ribeiro, F. *Catal. Today* **2007**, *123*, 224–234.

[29] Altman, E.; Gorte, R. *Surf. Sci.* **1986**, *172*, 71–80.

[30] Rashkeev, S. N.; Sohlberg, K.; Glazoff, M. V.; Novak, J.; Pennycook, S. J.; Pantelides, S. T. *Phys. Rev. B* **2003**, *67*, 115414.

[31] Mak, C.; George, S. *Chem. Phys. Lett.* **1987**, *135*, 381–386.

[32] Islam, M. M.; Calatayud, M.; Pacchioni, G. *J. Phys. Chem. C* **2011**, *115*, 6809–6814.

[33] Vittadini, A.; Casarin, M.; Selloni, A. *Theor. Chem. Acc.* **2007**, *117*, 663–671.

[34] Tilocca, A.; Selloni, A. *J. Chem. Phys.* **2003**, *119*, 7445–7450.

[35] Mills, G.; Jónsson, H. *Phys. Rev. Lett.* **1994**, *72*, 1124–1127.

[36] Mills, G.; Jónsson, H.; Schenter, G. K. *Surf. Sci.* **1995**, *324*, 305–337.

[37] Finnis, M.; Lozovoi, A.; Alavi, A. *Annu. Rev. Mater. Res.* **2005**, *35*, 167–207.

[38] Hine, N. D. M.; Frensch, K.; Foulkes, W. M. C.; Finnis, M. W. *Phys. Rev. B* **2009**, *79*, 024112.

[39] Kresse, G.; Hafner, J. *Phys. Rev. B* **1993**, *47*, 558–561.

[40] Kresse, G.; Hafner, J. *Phys. Rev. B* **1994**, *49*, 14251–14269.

[41] Kresse, G.; Furthmüller, J. *Comp. Mater. Sci.* **1996**, *6*, 15–50.

[42] Kresse, G.; Furthmüller, J. *Phys. Rev. B* **1996**, *54*, 11169–11186.

[43] Perdew, J. P.; Burke, K.; Ernzerhof, M. *Phys. Rev. Lett.* **1996**, *77*, 3865–3868.

[44] Perdew, J. P.; Burke, K.; Ernzerhof, M. *Phys. Rev. Lett.* **1997**, *78*, 1396.

[45] Sanville, E.; Kenny, S. D.; Smith, R.; Henkelman, G. *J. Comput. Chem.* **2007**, *28*, 899–908.

[46] Tilocca, A.; Selloni, A. *Langmuir* **2004**, *20*, 8379–8384.

[47] Tilocca, A.; Selloni, A. *J. Phys. Chem. B* **2004**, *108*, 47434751.

[48] Vittadini, A.; Selloni, A.; Rotzinger, F. P.; Grätzel, M. *Phys. Rev. Lett.* **1998**, *81*, 2954–2957.

[49] Henkelman, G.; Jónsson, H. *J. Chem. Phys.* **2000**, *113*, 9978.

[50] Sheppard, D.; Terrell, R.; Henkelman, G. *J. Chem. Phys.* **2008**, *128*.

[51] Aschauer, U. J.; Tilocca, A.; Selloni, A. *Int. J. Quantum Chem* **2015**, *2*, n/a–n/a.

[52] Burgess, D. R. Thermochemical Data, NIST Chemistry WebBook, NIST Standard Reference Database Number 69.

[53] Domalski, E. S.; Hearing, E. D. Condensed Phase Heat Capacity Data, NIST Chemistry WebBook, NIST Standard Reference Database Number 69.